Title
Revisiting the link between magnetic properties and chemisorption at graphene nanoribbon zigzag edge

Journal
The Journal of Chemical Physics, 156(4)

ISSN
0021-9606

Authors
Wei, Ziyang
Sautet, Philippe

Publication Date
2022-01-28

DOI
10.1063/5.0079064

Revisiting the Link between Magnetic Properties and Chemisorption at Graphene Nanoribbon Zigzag Edge

Ziyang Wei[†] and Philippe Sautet[*,†,‡]

[†]*Department of Chemistry and Biochemistry, University of California, Los Angeles, California, 90095, United States*

[‡]*Department of Chemical and Biomolecular Engineering, University of California, Los Angeles, California, 90095, United States*

E-mail: sautet@ucla.edu

Abstract

Graphene has received tremendous interest in both chemical and physical fields. Among the different edges of the graphene system, the zigzag edge terminated graphene nanoribbons (ZGNRs) show unique magnetic properties in the antiferromagnetic (AFM) state. However, to date the understanding of ZGNR chemical properties is mainly based on the partial radical concept and in the previous studies the energy differences between the ferromagnetic (FM) and AFM states are smaller than experimental evidence. Here, we report that the strongly constrained and appropriately normed functional gives a significantly larger energy difference which matches the experimental observation. Furthermore, utilizing the energetics in the large difference case, we propose a conceptual supplement to the previous partial radical concept: the overall stabilization of the AFM state compared to the nonmagnetic (NM) state consists of

two parts which affect the adsorption energy conversely. The NM-FM energy differences will strengthen the adsorption, being in line with the previous partial radical concept. The FM-AFM energy differences will instead weaken the adsorption. We perform calculations of H, OH, and LiS radical adsorption energies on ZGNRs to show that this weakening effect is numerically non-negligible: at least a ∼0.2 eV difference in the adsorption energies is found. We expect that this refinement of the partial radical concept can provide a more comprehensive understanding of chemical properties of ZGNRs. The differences in adsorption energies for H, OH, and LiS radicals found here lead to significant changes in the predicted reactivity of ZGNR models.

Introduction

Graphene has received a tremendous interest in both chemical and physical fields due to its various exceptional properties.[1–4] Edges of the two dimensional graphene share the same geometry with the one dimensional nanoribbons: cutting followed by saturation of the dangling σ bonds provides two different systems, armchair and zigzag edge terminated graphene nanoribbons. Edge-specific physics has been found on these systems as zigzag edge terminated graphene nanoribbons (ZGNR) introduce flat bands near the Fermi level and uniquely open the band gap in the antiferromagnetic (AFM) state,[5] as shown in Fig. 1 (c), and this AFM state becomes the groundstate. Such a flat band in related systems was firstly suggested by Kobayashi[6] for a zigzag-edged graphite in 1993 using the DV-Xα method and the linear combination of atomic orbitals bases, and independently by Klein[7] for several graphene ribbons with zigzag edges in 1994 using Hückel type model Hamiltonian. Later theoretical investigations agree on the appearance of the edge states and of an AFM coupling between the two edges of a ZGNR regardless of the methods used, varying from model Hamiltonians[5,8–13] to different exchange-correlation functionals.[14–18] Importantly, Nakada et al.[8] demonstrated that such an edge shape with three or four zigzag sites per sequence is sufficient to show an edge state, when the system size is on a nanometer scale. Recent

experiments[19–21] confirmed the band gap opening and the room-temperature AFM order on ZGNRs that are narrower than seven nanometers,[19] suggesting a further stabilization of the AFM state: computational results using hybrid functionals only predict the room-temperature AFM order to exist within the ribbon width of one to two nanometers.[17]

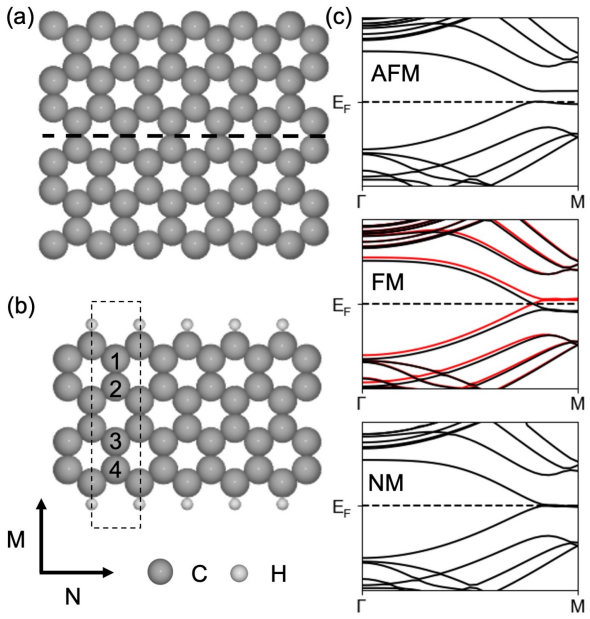

Figure 1: (a) The direction of cutting through an infinite graphene terrace to create the zigzag edge, denoted by the dashed line. (b) Zigzag edge nanoribbon models used in this study with a $N \times M$ notation. The edge carbon atoms are saturated with hydrogen atoms. C atoms are shown as grey, and H atoms white. N and M are the numbers of the carbon atoms across the length and width in the cell, respectively. Numbers on the atoms count the M=4 width of the model shown here and the cell labeled by the dashed line is denoted as a 1×4 cell. (c) The band structure of the AFM, FM, and NM states.[17] For the FM state, the black and red curves indicate the major and minor spin components, respectively.

Aside from the physical properties such as electronic structures and magnetic properties, the graphene system has attracted considerable interest from the field of the electrocatalysis as well.[22] Success with this system has been achieved for hydrogen evolution reaction[23,24] (HER), oxygen reduction reaction[25,26] (ORR), and sulfur reduction reaction[27] (SRR). However, to date the understanding of ZGNR chemical properties is mainly based on the partial radical concept proposed by Jiang et al.:[18] in the aforementioned AFM states, the unpaired π electrons distributed on the edge atoms offer special chemical reactivity. Compared with

the terrace carbon atoms, armchair carbon atoms, or nanotube carbon atoms, where the adsorption is too weak, the unpaired electron densities on edge carbon atoms make the adsorption of intermediates more favored. These edge carbon atoms in ZGNRs show similarity to common radical species and hence are called partial radicals. Nevertheless, in ZGNRs, the ferromagnetic (FM) state, which is a metastable state, also serves as partial radicals: the local magnetic moments on edge carbon atoms in the FM state are comparable with the ones in the AFM state.[18] Essentially, the partial radical nature comes from the stabilization compared to the nonmagnetic (NM) state, i.e., a large NM-AFM or FM-NM energy difference. The previous work of Jiang et al.[18] used the Perdew-Burke-Ernzerhof (PBE) functional[28] and the results rely on the PBE energetics, which gives relatively small FM-AFM energy differences, ca. one fifth compared to the FM-NM energy differences. Experimentally observed room-temperature AFM order in ZGNRs indicates an FM-AFM energy difference which is one magnitude larger than the value obtained using hybrid functionals, which is already larger than the PBE values by one magnitude.[17]

In this work we aim to refine the concept of ZGNR as partial radical systems. We first show that significantly larger FM-AFM energy differences are achieved with the strongly constrained and appropriately normed (SCAN) functional[29] compared to other local spin density approximation[30] (LSDA), generalized gradient approximation (GGA), metaGGA and hybrid functionals. We show that the large FM-AFM energy difference is in line with the experimental results, the room-temperature AFM order at the width of ca. 7 nm.[19] We then propose a refinement of the partial radical concept based on the adsorption energetics of three radicals, H, OH, and LiS, representing three different types of electrochemical reactions: HER,[31] ORR,[32] and SRR.[27] We found that the stability of the AFM state with respect to the FM state, i.e., large FM-AFM energy difference, will lead to a weakening of the adsorption energy. This is a supplement to the partial radical concept proposed by Jiang et al.[18] which focused on the stabilization of partial radical states with respect to the NM state, i.e., the NM-FM energy differences, which will strengthen the adsorption and explained the

stronger adsorption with respect to close shell C atoms such as terrace C atoms in graphene. Our results stress the importance of the ratio between the NM-FM and FM-AFM energy differences, which affect the adsorption energies conversely. Our results also suggest that the SCAN functional provides a valuable chance to investigate the large FM-AFM energy difference case, which is in line with the experimental results.

Methods

DFT calculations

The Vienna Ab initio Simulation Package[33] (VASP) was used for calculations. We utilized different DFT exchange correlation functionals including the LSDA , PBE,[28] SCAN,[29] Tao-Perdew-Staroverov-Scuseria (TPSS),[34] Becke-3-Lee-Yang-Parr (B3LYP),[35] PBE0,[36] and Heyd-Scuseria-Ernzerhof (HSE06)[37] functionals. All the DFT calculations were developed on a basis set of plane waves with a cutoff energy as 500 eV. Core electrons were described with the projector augmented wave (PAW) method. A gaussian smearing with sigma value of 0.1 eV was used through all calculations. For self consistent calculations, an electronic step convergence criterion of 10^{-6} eV were used. Structural convergence was assumed for forces lower than 0.02 eV/Å and geometry optimizations were performed for the PBE, SCAN and TPSS functionals. Single point energies were reported for hybrid functionals based on PBE geometries.

For the ZGNR models, the in plane and out plane vacuum between the ribbons were set as 15Å. The PBE value of C-C bond length of graphene, 1.424 Å, which is consistent with the experimental value 1.42 Å, was used for all the models. We name the ZGNR models with a $N \times M$ notation, where N and M are the numbers of the carbon atoms across the length and width in the cell, respectively, as shown in Fig. 1. For the $1 \times M (M = 2\ to\ 8)$ models on which the calculations of FM-AFM energy differences were performed, a 15×1×1 k-point mesh was used. For the $4 \times M$ and $5 \times M$ $(M = 4, 5, 6)$ models on which the adsorption

energy calculations were performed, a 3×1×1 k-point mesh was used and further test details are provided in the SI, table S1. We have performed test calculations with a 6×1×1 k-point mesh and found the uncertainty to be within 30 meV. It is worth mentioning that the width of each model before relaxation, starting and ending at edge C atoms, is $0.712 + 2.136M$ Å. The reference energies of H, OH, and LiS radicals are calculated as an isolated radical placed in a 15×16×17×box with a $\mathbf{\Gamma}$ point only k-point mesh. We choose this radical reference to avoid differences between the chemical reaction energies of various functionals used, e.g., the reference of OH radical using H_2 and H_2O involves the bond dissociation energies of these two molecules.

Models with $N = 4, 5$ and $M = 4, 5, 6$ were used for adsorption energy calculations. Models with $N = 4, 5$ give a reasonable coverage from 1/4 to 1/5. Models with $M = 4, 5, 6$ correspond to a width over 1 nm while being affordable for hybrid functionals. The adsorption energy calculations were performed with all the functionals other than LSDA since LSDA is not widely used to describe the chemical properties. We show the results of models with $N = 5$ in the main text and the results of $N = 4$ are provided in the SI, Fig. S1. The difference in the length, N, of the models only leads to small quantitative differences and no qualitative distinction.

Results and Discussion

FM-AFM Energy Difference

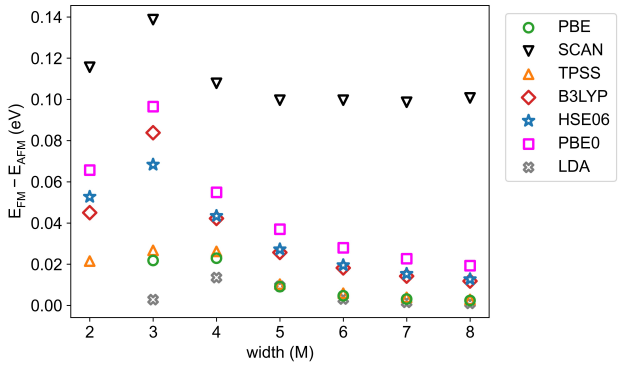

Figure 2: The FM-AFM energy difference, defined as $E_{edge,FM} - E_{edge,AFM}$, using different functionals per $1 \times M$ cell with $M = 2$ *to* 8. The LSDA and PBE data points are not shown for $M = 2$ as LSDA and PBE functionals fail to achieve the AFM/FM and FM states at the width of $M = 2$.

The band structures of the three magnetic states, the AFM, FM, and NM states (an example for our 1×4 model is given in Fig. 1 (c)) has been well studied using different methods including model Hamiltonians, LSDA, DFT-GGA, and hybrid functionals. We do not focus on these aspects as our band structures and the general energetic order as $E_{AFM} < E_{FM} < E_{NM}$ are in line with the previous studies. We start with the FM-AFM energy difference, defined as $E_{edge,FM} - E_{edge,AFM}$, using different functionals and the results of $1 \times M$ ($M = 2$ *to* 8) ZGNR models are shown in Fig. 2. At the width of M=2, the FM-AFM energy difference is not shown for LSDA and PBE as we can only achieve the NM state for LSDA and the NM and FM states for PBE. Among all the functionals tested, the LSDA functional gives the smallest FM-AFM energy difference, i.e., the weakest AFM stabilization, with a maximum of 0.013 eV per unit cell appearing at the width of M=4 followed by a monotonic decrease. The PBE functional gives the second smallest FM-AFM energy differences, with a maximum of 0.023 eV at the width of M=4 followed by a monotonic decrease. Among the functionals that give FM-AFM energy difference at the width of M=2 (TPSS, B3LYP, HSE06, PBE0),

the TPSS functional provides a smallest FM-AFM with the maximum value of 0.027 eV at the width of M=3. Results of the three hybrid functionals, B3LYP, HSE06, and PBE0, are similar to each other while the energy differences are significantly larger than the LSDA, PBE and TPSS results. The monotonic decrease is observed for M$\geqslant$3 and the maximum values are 0.084, 0.068, and 0.096 eV for the B3LYP, HSE06, and PBE0 functionals, respectively. For all the widths of M$\geqslant$4 the order is found to be B3LYP<HSE06<PBE0. The SCAN functional gives the largest FM-AFM energy difference with a maximum of 0.144 eV at the width of M=3 followed by a monotonic decrease until M=5, and then a rather constant value up to M=8. The difference between the SCAN and other functionals becomes more significant at large widths (M>6), where the SCAN values are ca. 5 to 10 times larger than that of the hybrid functionals. The stabilization of the AFM state is in line with the strong magnetic tendencies of the SCAN functional in metals[38] and may come from the fact that the SCAN functional, like the hybrid functionals, is implemented in a generalized Kohn-Sham scheme in which the exchange-correlation potential is not a multiplicative operator.[39]

The increasing order of the FM-AFM energy difference LSDA<PBE<TPSS<hybrid functionals<SCAN is interesting. The general order LSDA<GGA<metaGGA<hybrid functionals, except the SCAN functional, is in line with the fact that a larger extent of localization leads to more significant stabilization of the AFM state.[17] This also explains why LSDA and PBE functionals fail to achieve the AFM/FM and FM states at the width of M=2: the electrons are delocalized too much for LSDA so that both magnetic states cannot be stabilized whereas PBE has a similar but less severe problem, and is unable to define the FM state. The LSDA and PBE functionals give the maximum energy difference at the width of M=4, whereas all the other functionals give the largest difference at the width of M=3: the magnetic tails of the edge states in PBE and LSDA are more delocalized and therefore the maximum interaction strength is reached at a larger width as well. It is not surprising that the SCAN functional gives larger FM-AFM energy differences compared to other LSDA, GGA, and metaGGA functionals: for the ferromagnetic systems, the SCAN functional is

known to give significantly more stable FM states with respect to NM states compared to the results of LSDA, PBE, TPSS and revTPSS functionals.[40] The fact that the SCAN functional gives five to ten times more stabilization of the AFM state compared with hybrid functional is surprising while intriguing as experimental results suggest a energy difference larger than the B3LYP one by one magnitude: the relationship between the FM-AFM energy difference and the width of ZGNRs has been shown to be:

$$E \propto W^n \tag{1}$$

where E denotes the FM-AFM energy difference, W denotes the width of the ZGNR model while our model with a $N \times M$ notation is estimated to have a width of 0.712+2.136M Å, and n is the power number, either fitted for different functionals, ranging from -1.39 for LSDA to -1.82 for B3LYP,[17] or shown to be -2 for different model Hamiltonians.[12,13] Our hybrid functional results matches well with the results of Pisani et al.,[17] showing a $\sim kT$ energy difference around 1-2 nm. However, to achieve an AFM order at 7 nm, a 3.5^2 to 7^2, i.e., ca. 10 to 50 times larger energy difference is required and results of the SCAN functional serve this purpose well. Moreover, deviations from the ideal edge structure can be present on the experimental materials and such defects and impurities will generally weaken the AFM order, thus the experimental observed 7 nm should be treated as the lower limit for the computational non-defected models to match, further stressing the importance to have a large FM-AFM energy difference at the magnitude that the SCAN functional gives.

Adsorption Energy of H, OH, and LiS radicals

We have shown that the SCAN functional gives a significantly larger stabilization of the AFM state agreeing with the experimental observations. We then check the local magnetic moments on the edge carbon atoms, which are in link with the partial radical concept proposed by Jiang et al.:[18] in both the AFM and FM states, the spin-polarized π electrons

are localized on the edge carbon atoms, as shown in Table 1. (The values using other functionals are provided in the SI, Table S2. The TPSS results are similar to the PBE results. The B3LYP and HSE06 results are slightly smaller than the PBE0 results.)

Table 1: Local magnetic moments on the edge carbons of the ferromagnetic states, M_{FM}, and antiferromagnetic states, M_{AFM}, in the $1 \times M$ models ($M = 4, 5, 6$) using different functionals. All values are in the unit of Bohr magneton, μ_B. Results of the PBE, SCAN, and PBE0 functionals are shown.

Width (M)	$M_{FM,PBE}(\mu_B)$	$M_{FM,SCAN}(\mu_B)$	$M_{FM,PBE0}(\mu_B)$
4	0.130	0.182	0.170
5	0.144	0.190	0.173
6	0.145	0.191	0.176
Width (M)	$M_{AFM,PBE}(\mu_B)$	$M_{AFM,SCAN}(\mu_B)$	$M_{AFM,PBE0}(\mu_B)$
4	0.141	0.200	0.188
5	0.147	0.204	0.188
6	0.148	0.202	0.187

Our local magnetic moment values using the PBE functional agree well with the previous results of Jiang et al.[18] Consistent with the stabilization of the AFM state, the SCAN functional predicts larger local magnetic moments than the PBE functional, and even the hybrid functionals, i.e., the largest local magnetic moments among the functionals tested. It is worth mentioning that the SCAN and PBE0 results are closer to the Hubbard model results ($M = 10, U/t = 0.1$): a local magnetic moment of 0.19 μ_B, as published by Fujita et al.[5] These results naturally motivate us to check the influence of these magnetic properties on the adsorption energies of different radicals: according to the partial radical concept, the stronger partial radical nature given by the SCAN functional should correspond to a stronger adsorption.

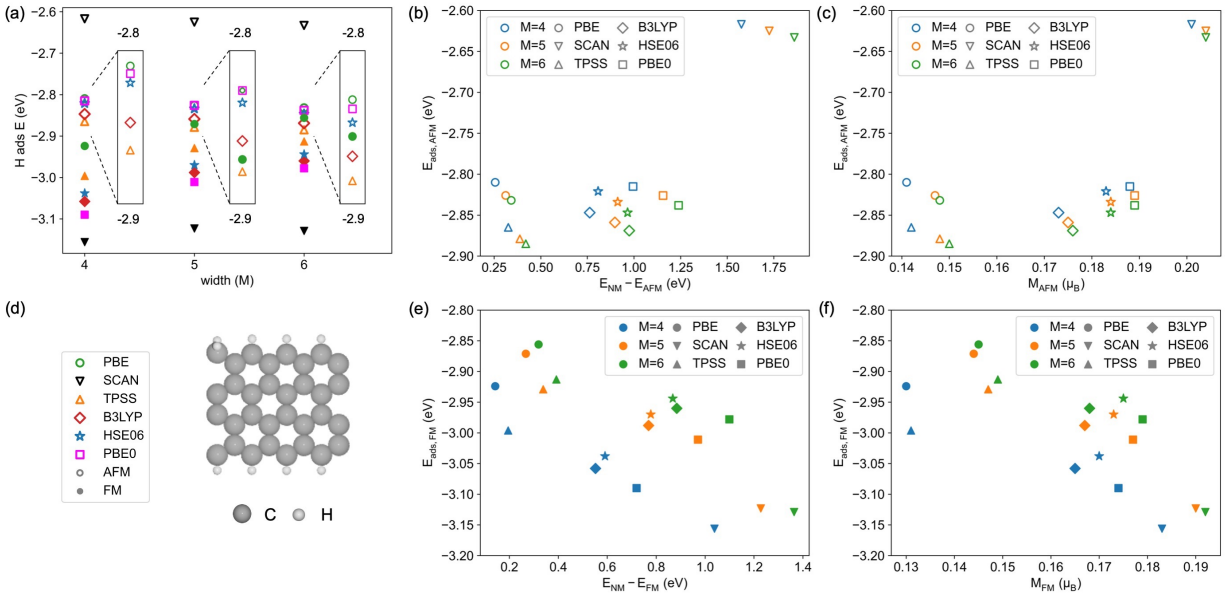

Figure 3: (a) The adsorption energies of H radical on $5 \times M$ ZGNR models using the PBE, SCAN, TPSS, B3LYP, HSE06, and PBE0 functionals. Open symbols indicate the physical adsorption energy, calculated with respect to the most stable AFM state of the ZGNR, $E_{ads,AFM} = E_{edge+H} - E_{edge,AFM} - E_H$, and filled symbols indicate the hypothetical adsorption energy, calculated with respect to the metastable FM state of the ZGNR, $E_{ads,FM} = E_{edge+H} - E_{edge,FM} - E_H$. Details of energetics within the range of -2.9 to -2.8 eV are shown in the inset to the right. (b) and (c) The relationship between the adsorption energy $E_{ads,AFM}$ and (b) $E_{edge,NM} - E_{edge,AFM}$, and (c) M_{AFM}. (d) The top view of the atomic structure of adsorbed H on a 5×4 ZGNR model and the legend of (a). C atoms are shown as grey, and H atoms white. (e) and (f) The relationship between the adsorption energy $E_{ads,FM}$ and (b) $E_{edge,NM} - E_{edge,FM}$, and (c) M_{FM}. In (a) the colors together with the shapes indicate the functionals used. In (b), (c), (e), and (f) the colors indicate the width of the models used and the shapes indicate the functionals used.

We firstly check the adsorption energy of the H radical. Our PBE results agrees well with the results of Jiang et al.[18] at 1/6 coverage, indicating a good approximation to the low coverage limit. Surprisingly, SCAN gives the weakest instead of the strongest adsorption energies, $E_{ads,AFM} = E_{edge+radical} - E_{edge,AFM} - E_{radical}$, among all the functional tested, shown as filled circles in Fig. 3 (a). The disobedience from the aforementioned partial radical concept is rather significant: instead of having the most negative adsorption energy, the SCAN functional predicts adsorption energies, -2.617 eV to -2.633 eV, being more positive by ca. 0.2 eV compared to the functional giving the second least favorable energy (PBE).

This disobedience motivates us to consider other aspects of the adsorption energy. As we have mentioned previously, the FM state also shows partial radical character, and subsequently a hypothetical adsorption energy can be defined as $E_{ads,FM} = E_{edge+radical} - E_{edge,FM} - E_{radical}$, shown as triangles in Fig. 3 (a). Note this hypothetical adsorption energy is linked with the physical adsorption energy via the addition of the FM-AFM energy difference, $(E_{edge,FM} - E_{edge,AFM})_{1\times M}$, as shown in Fig. 2, multiplied by the length of the model, N:

$$\begin{aligned} E_{ads,AFM} &= E_{edge+radical} - E_{edge,AFM} - E_{radical} \\ &= E_{edge+radical} - E_{edge,FM} - E_{radical} + E_{edge,FM} - E_{edge,AFM} \\ &= E_{ads,FM} + (E_{edge,FM} - E_{edge,AFM})_{N\times M} \\ &= E_{ads,FM} + N \times (E_{edge,FM} - E_{edge,AFM})_{1\times M} \end{aligned} \tag{2}$$

Interestingly, the SCAN functional gives the most negative value for the hypothetical $E_{ads,FM}$, -3.156 eV to -3.129 eV across the widths of $M = 4, 5, 6$, slightly more negative than the hybrid functionals as PBE0: -3.090 eV to -2.978 eV. Moreover, the results achieved with different functionals allow us to compare the radical character using two different descriptors: (1) the stabilization of magnetic states with respect to the non-magnetic states, i.e., $E_{edge,NM} - E_{edge,AFM}$ and $E_{edge,NM} - E_{edge,FM}$. (2) the local magnetic moments on the edge carbon atoms, i.e., M_{AFM} and M_{FM}. For both descriptors, we found no simple trend for the AFM properties, i.e., $E_{ads,AFM}$ with respect to $E_{edge,NM} - E_{edge,AFM}$ or M_{AFM}, as shown in Fig. 3 (b) and (c); on the other hand, the correlation is found to be obvious with respect to the FM properties, i.e., $E_{ads,FM}$ with respect to $E_{edge,NM} - E_{edge,FM}$ or M_{FM}, as shown in Fig. 3 (e) and (f). For every specific model width in Fig. 3 (e) and (f), $E_{edge,NM} - E_{edge,FM}$ is found to be linearly correlated with the $E_{ads,FM}$. These results suggest that we cannot directly correlate the AFM state stabilization, $E_{edge,NM} - E_{edge,AFM}$, with the adsorption energy. Instead, correlations are better found for the FM state stabilization and it explains why we failed to correlate the $E_{ads,AFM}$ with $E_{edge,NM} - E_{edge,AFM}$: as shown in Eq. 2, the $E_{ads,AFM}$ consists of the hypothetical adsorption energy, $E_{ads,FM}$, and the stabilization of

the AFM state with respect to the FM state, $E_{edge,FM} - E_{edge,AFM}$. This also explains why the energy difference of the FM and AFM states, $E_{edge,FM} - E_{edge,AFM}$, is related with the weakening of the adsorption: this term is added into instead of subtracted from the physical adsorption energy, $E_{ads,AFM}$. Moreover, the first term is found to be correlated with $E_{edge,NM} - E_{edge,FM}$, which adds up with the second term, $E_{edge,FM} - E_{edge,AFM}$, into the overall stabilization of the AFM state, $E_{edge,NM} - E_{edge,AFM}$:

$$E_{edge,NM} - E_{edge,AFM} = (E_{edge,NM} - E_{edge,FM}) + (E_{edge,FM} - E_{edge,AFM}) \quad (3)$$

The complicated trend of $E_{ads,AFM}$ with respect to $E_{edge,NM} - E_{edge,AFM}$ comes from the fact that these two components affects the adsorption energy conversely. The previous study of Jiang et al.[18] focus more on the limit of small FM-AFM energy difference, which is given by the PBE energetics: in that situation, the overall stabilization of the AFM state, $E_{edge,NM} - E_{edge,AFM}$ is quite close to the stabilization of the FM state, $E_{edge,NM} - E_{edge,FM}$ and generally a stronger radical character will simply lead to a more negative adsorption energy. However, as the FM-AFM energy difference implied by experiments is considerably larger, the influence of the FM-AFM energy difference should not be neglected. The SCAN functional provides the chance to look into this case and predicts a $\sim$0.2 eV weakening of the H radical adsorption.

To ensure these findings are general, we further perform calculations for OH and LiS radicals, as shown in the Fig. 4 (a) and (b), respectively. The relationship between $E_{ads,FM}$ and $E_{edge,NM} - E_{edge,FM}/M_{FM}$ is provided in the SI, Fig. S2. It is not surprising that due to the increased complexity of the radicals, the adsorption energies are no longer only dictated by the partial radical character. The PBE functional gives more negative values of $E_{ads,FM}$ for the OH and LiS adsorption and the B3LYP functional gives more positive value of $E_{ads,FM}$ for the LiS radical adsorption, compared to the trend predicted by the partial radical character. Nevertheless the TPSS, SCAN, HSE06 and PBE0 functionals (i.e., two

hybrid functionals following the exchange fraction argument based on adiabatic connection formula[41]) still generally follow the trend. The adsorption energies of the SCAN functional still appear to be weaker than HSE06 and PBE0 results by ∼0.2 eV and only in the LiS adsorption case, is not the weakest among all the functionals tested. Moreover, the difference between the SCAN and PBE results appears to be rather significant: 0.4-0.6 eV in the case of OH and LiS adsorption.

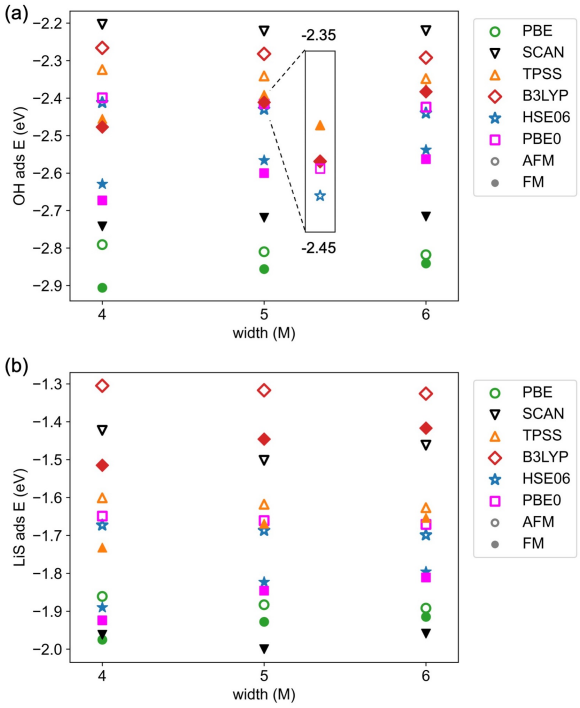

Figure 4: The adsorption energies of (a) OH and (b) LiS radicals on $5 \times M$ ZGNR models using the PBE, SCAN, TPSS, B3LYP, HSE06, and PBE0 functionals. Open symbols indicate the physical adsorption energy, calculated with respect to the most stable AFM state of the ZGNR, $E_{ads,AFM} = E_{edge+OH/LiS} - E_{edge,AFM} - E_{OH/LiS}$, and filled symbols indicate the hypothetical adsorption energy, calculated with respect to the metastable FM state of the ZGNR, $E_{ads,FM} = E_{edge+OH/LiS} - E_{edge,FM} - E_{OH/LiS}$. In (a), details of energetics of the model with width as $M = 5$ within the range of -2.45 to -2.35 eV are shown in the inset.

All these results suggest that the influence of the unique physical property of ZGNRs, i.e., the stability of the AFM state, on chemical adsorption energies can be decomposed into two components: (1) the stabilization of the FM state with respect to the NM state, (2) the stabilization of the AFM state with respect to the FM state. These two components

affect the adsorption energy conversely. (1) A stronger FM state stabilization is found to be correlated with a more negative hypothetical adsorption energy $E_{ads,FM}$. This is the intuitive relationship as a stronger radical character leads to stronger adsorption. (2) A stronger AFM state stabilization with respect to the FM state is found to be correlated with a more positive adsorption energy. Whether a larger NM-AFM energy difference, i.e., a partial radical character in the AFM form, leads to a stronger adsorption of radicals depends on the ratio of these two components. The experimental evidence suggest that the FM-AFM energy difference is significant: the observed room-temperature AFM order implies a ca. 10 to 50 time larger FM-AFM energy difference compared to the hybrid functional results at the width of 1-2 nm, and the SCAN functional results match this well. Therefore, the large FM-AFM energy difference suggests a clear weakening of the adsorption energy: $\sim$0.2 eV compared to hybrid functionals like HSE06 and PBE0, and even larger weakening compared to the PBE functional. Consequently the results suggest a cautious interpretation of the PBE results on ZGNRs, as the unique property, the FM-AFM energy difference, is found to be rather small with the PBE functional compared to the experimental data.

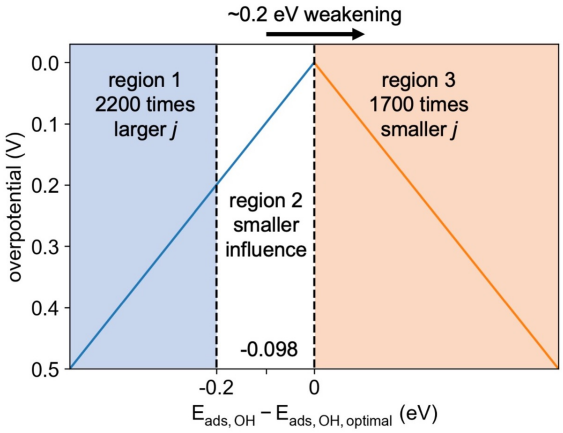

Figure 5: The influence of this ∼0.2 eV adsorption energy weakening on the current density in electrocatalytic systems, shown for the exemplary volcano plot of the ORR system using the current-adsorption energy relationship proposed by Nørskov et al.[42] The strong and weak binding legs are shown as blue and orange lines, respectively. Three regions with different influences are separated by the vertical dashed lines. The blue shade indicates region 1 where current density will be ∼2200 times larger due to this weakening. The orange shade indicates region 3 where current density will be ∼1700 times larger due to this weakening. Non-shaded part corresponds to region 2 where the influence is relatively smaller compared to region 1 and 3: at the point of $E_{ads,OH} - E_{ads,OH,opt}$=-0.098 eV, the current density remains the same after applying this weakening; when the $E_{ads,OH}$ deviates from the value, the influence grows exponentially.

This ∼0.2 eV imposes significant influences on the reaction activity of electrocatalytic sites: Sabatier principle states that the optimal catalytic site is achieved when the adsorption energy of the key intermediates, known as the descriptor, is neither too strong nor too weak. The adsorption energies of H,[43] OH,[42,44] and LiS[27] radicals have been utilized as descriptors for HER, ORR, and SRR, respectively. We estimate the influence of this ∼0.2 eV weakening of adsorption energy using ORR as an example. On the strong binding (left) leg of the volcano plot, as shown in Fig. 5, the relationship between the current density and OH adsorption energy has been shown to be:[42]

$$kTln(\frac{j}{j_{optimal}}) = E_{ads,OH} - E_{ads,OH,optimal} \tag{4}$$

where the j and $E_{ads,OH}$ are current density and the OH radical adsorption energy of a

specific site, $j_{optimal}$ and $E_{ads,OH,optimal}$ is the current density and the OH radical adsorption energy of the hypothetical perfect system at the top of this volcano plot.

Similarly, with the fitted parameter α to be 0.97, on the weak binding (right) leg, the relationship has been shown to be:

$$kTln(\frac{j}{j_{optimal}}) = \alpha * (E_{ads,OH,optimal} - E_{ads,OH}) \tag{5}$$

The influence of this weakening is found to be rather significant. As shown in Fig. 5, in region 1, where the adsorption energy is too strong without this effect, the sites will be pushed closer to the top and the current will $e^{\frac{0.2}{0.026}} \approx 2200$ times larger. Similarly in region 3, all the sites will be pushed away from the top and the current will be $e^{\frac{0.97*0.2}{0.026}} \approx 1700$ times smaller. Only around the point where $E_{ads,OH,opt} - E_{ads,OH} = 0.97 * (E_{ads,OH} + 0.2 - E_{ads,OH,opt})$, i.e., the adsorption energy being 0.098 eV stronger than the top of the volcano plot, the influence will be small, but still grows exponentially when the adsorption energy deviates from this value. These analyses clearly show that for electrocatalytic systems, this ∼0.2 eV weakening will introduce a significant effect for catalytic sites in a wide range of adsorption energy, ∼2000 times larger or smaller current depending on the detailed adsorption strength.

Conclusion

In this work we explore the electronic structure, magnetism and chemisorption properties of graphene nanoribbons presenting the zigzag edge. One aim is to refine the partial radical concept of the ZGNRs. We first show that significantly larger FM-AFM energy differences at the zigzag edge are achieved with the SCAN functional compared with other functionals. We show that the large FM-AFM energy difference is in line with the experimental results, the room-temperature AFM order at the ribbon width of ca. 7 nm. We then describe the unique role of the FM-AFM energy difference: instead of strengthening the adsorption, the AFM groundstate is found to weaken the adsorption. The two components in the overall

stability of the AFM state, the NM-AFM energy difference, affect the chemical adsorption energy conversely: a larger FM-AFM energy difference weakens the adsorption strength whilst a larger NM-FM energy difference strengthens it. We validate this trend with the adsorption of three radicals, H, OH, and LiS, as the adsorption energies are widely used as descriptor for three different types of electrochemical reactions: HER, ORR, and SRR. We expect the weakening effect, which is described incompletely by the other functionals due to the small FM-AFM energy differences, to give at least a $\sim$0.2 eV difference in the adsorption energies on ZGNRs. This difference imposes significant effects on the predicted reactivity on that edge of graphene nanoribbons for HER, ORR, and SRR: $\sim$2000 times larger or smaller current density depending on the detailed adsorption strength.

Supplementary Material

K-point Mesh Influence on Adsorption Energies (Table S1); Energetics of the $4 \times M$ Models (Fig. S1); Local Magnetic Moments on the Edge Carbons Using Different Functionals (Table S2); Relationship between OH/LiS Radical Adsorption Energies and Partial Radical Features (Fig. S2)

Acknowledgement

This work is supported by the Center for Synthetic Control Across Length-scales for Advancing Rechargeables, an Energy Frontier Research Center funded by the US Department of Energy, Office of Science Basic Energy Sciences programme under award DE-SC0019381. The calculations were performed on the Hoffman2 cluster at UCLA Institute for Digital Research and Education (IDRE) and the Extreme Science and Engineering Discovery Environment (XSEDE),[45] which is supported by National Science Foundation grant number ACI-1548562, through allocation TG-CHE170060.

References

(1) Castro Neto, A.; Guinea, F.; Peres, N.; Novoselov, K.; Geim, A. The electronic properties of graphene. *Rev. Mod. Phys.* **2009**, *81*, 109–162.

(2) Allen, M. J.; Tung, V. C.; Kaner, R. B. Honeycomb Carbon: A Review of Graphene. *Chem. Rev.* **2009**, *110*, 132–145.

(3) Novoselov, K.; Falko, V.; Colombo, L.; Gellert, P.; Schwab, M.; Kim, K. A roadmap for graphene. *Nature* **2012**, *490*, 192–200.

(4) Grigorenko, A.; Polini, M.; Novoselov, K. Graphene plasmonics. *Nature Photon* **2012**, *6*, 749–758.

(5) Fujita, M.; Wakabayashi, K.; Nakada, K.; Kusakabe, K. Peculiar Localized State at Zigzag Graphite Edge. *J. Phys. Soc. Jpn.* **1996**, *65*, 1920–1923.

(6) Kobayashi, K. Electronic structure of a stepped graphite surface. *Phys. Rev. B* **1993**, *48*, 1757–1760.

(7) Klein, D. Graphitic polymer strips with edge states. *Chem. Phys. Lett.* **1994**, *217*, 261–265.

(8) Nakada, K.; Fujita, M.; Dresselhaus, G.; Dresselhaus, M. S. Edge state in graphene ribbons: Nanometer size effect and edge shape dependence. *Phys. Rev. B* **1996**, *54*, 17954–17961.

(9) Wakabayashi, K.; Fujita, M.; Ajiki, H.; Sigrist, M. Electronic and magnetic properties of nanographite ribbons. *Phys. Rev. B* **1999**, *59*, 8271–8282.

(10) Yamashiro, A.; Shimoi, Y.; Harigaya, K.; Wakabayashi, K. Spin-and charge-polarized states in nanographene ribbons with zigzag edges. *Phys. Rev. B* **2003**, *68*, 193410.

(11) Sasaki, K.; Murakami, S.; Saito, R. Stabilization mechanism of edge states in graphene. *Appl. Phys. Lett.* **2006**, *88*, 113110.

(12) Jung, J.; Pereg-Barnea, T.; MacDonald, A. Theory of Interedge Superexchange in Zigzag Edge Magnetism. *Phys. Rev. Lett.* **2009**, *102*, 227205.

(13) Jung, J. Nonlocal exchange effects in zigzag-edge magnetism of neutral graphene nanoribbons. *Phys. Rev. B* **2011**, *83*, 165415.

(14) Kawai, T.; Miyamoto, Y.; Sugino, O.; Koga, Y. Graphitic ribbons without hydrogen-termination: Electronic structures and stabilities. *Phys. Rev. B* **2000**, *62*, R16349–R16352.

(15) Lee, H.; Son, Y.-W.; Park, N.; Han, S.; Yu, J. Magnetic ordering at the edges of graphitic fragments: Magnetic tail interactions between the edge-localized states. *Phys. Rev. B* **2005**, *72*, 174431.

(16) Son, Y.-W.; Cohen, M. L.; Louie, S. G. Half-metallic graphene nanoribbons. *Nature* **2006**, *444*, 347–349.

(17) Pisani, L.; Chan, J.; Montanari, B.; Harrison, N. Electronic structure and magnetic properties of graphitic ribbons. *Phys. Rev. B* **2007**, *75*, 064418.

(18) Jiang, D.-e.; Sumpter, B. G.; Dai, S. Unique chemical reactivity of a graphene nanoribbon's zigzag edge. *J. Chem. Phys.* **2007**, *126*, 134701.

(19) Magda, G. Z.; Jin, X.; Hagymási, I.; Vancsó, P.; Osváth, Z.; Nemes-Incze, P.; Hwang, C.; Biró, L. P.; Tapasztó, L. Room-temperature magnetic order on zigzag edges of narrow graphene nanoribbons. *Nature* **2014**, *514*, 608–611.

(20) Ruffieux, P.; Wang, S.; Yang, B.; Sánchez-Sánchez, C.; Liu, J.; Dienel, T.; Talirz, L.; Shinde, P.; Pignedoli, C. A.; Passerone, D.; Dumslaff, T.; Feng, X.; Müllen, K.; Fasel, R.

On-surface synthesis of graphene nanoribbons with zigzag edge topology. *Nature* **2016**, *531*, 489–492.

(21) Li, Y.; Chen, M.; Weinert, M.; Li, L. Direct experimental determination of onset of electron–electron interactions in gap opening of zigzag graphene nanoribbons. *Nat Commun* **2014**, *5*, 1–8.

(22) Deng, D.; Novoselov, K.; Fu, Q.; Zheng, N.; Tian, Z.; Bao, X. Catalysis with two-dimensional materials and their heterostructures. *Nature Nanotech* **2016**, *11*, 218–230.

(23) Jiao, Y.; Zheng, Y.; Davey, K.; Qiao, S.-Z. Activity origin and catalyst design principles for electrocatalytic hydrogen evolution on heteroatom-doped graphene. *Nat Energy* **2016**, *1*, 1–9.

(24) Xia, Z. Hydrogen evolution: Guiding principles. *Nat Energy* **2016**, *1*, 1–2.

(25) Li, M.; Zhang, L.; Xu, Q.; Niu, J.; Xia, Z. N-doped graphene as catalysts for oxygen reduction and oxygen evolution reactions: Theoretical considerations. *J. Catal.* **2014**, *314*, 66–72.

(26) Kulkarni, A.; Siahrostami, S.; Patel, A.; Nørskov, J. K. Understanding Catalytic Activity Trends in the Oxygen Reduction Reaction. *Chem. Rev.* **2018**, *118*, 2302–2312.

(27) Peng, L. et al. A fundamental look at electrocatalytic sulfur reduction reaction. *Nat Catal* **2020**, *3*, 762–770.

(28) Perdew, J. P.; Burke, K.; Ernzerhof, M. Generalized Gradient Approximation Made Simple. *Phys. Rev. Lett.* **1996**, *77*, 3865–3868.

(29) Sun, J.; Ruzsinszky, A.; Perdew, J. P. Strongly Constrained and Appropriately Normed Semilocal Density Functional. *Phys. Rev. Lett.* **2015**, *115*, 036402.

(30) Perdew, J.; Zunger, A. Self-interaction correction to density-functional approximations for many-electron systems. *Phys. Rev. B* **1981**, *23*, 5048–5079.

(31) Nørskov, J.; Bligaard, T.; Logadottir, A.; Kitchin, J.; Chen, J.; Pandelov, S.; Stimming, U. Trends in the Exchange Current for Hydrogen Evolution. *J. Electrochem. Soc.* **2005**, *152*, J23.

(32) Nørskov, J.; Rossmeisl, J.; Logadottir, A.; Lindqvist, L.; Kitchin, J.; Bligaard, T.; Jónsson, H. Origin of the Overpotential for Oxygen Reduction at a Fuel-Cell Cathode. *J. Phys. Chem. B* **2004**, *108*, 17886–17892.

(33) Kresse, G.; Hafner, J. Ab initio molecular dynamics for liquid metals. *Phys. Rev. B* **1993**, *47*, 558.

(34) Tao, J.; Perdew, J. P.; Staroverov, V. N.; Scuseria, G. E. Climbing the Density Functional Ladder: Nonempirical Meta–Generalized Gradient Approximation Designed for Molecules and Solids. *Phys. Rev. Lett.* **2003**, *91*, 146401.

(35) Becke, A. D. Density-functional thermochemistry. III. The role of exact exchange. *J. Chem. Phys.* **1993**, *98*, 5648–5652.

(36) Ernzerhof, M.; Scuseria, G. E. Assessment of the Perdew–Burke–Ernzerhof exchange-correlation functional. *J. Chem. Phys.* **1999**, *110*, 5029–5036.

(37) Krukau, A. V.; Vydrov, O. A.; Izmaylov, A. F.; Scuseria, G. E. Influence of the exchange screening parameter on the performance of screened hybrid functionals. *J. Chem. Phys.* **2006**, *125*, 224106.

(38) Fu, Y.; Singh, D. J. Applicability of the Strongly Constrained and Appropriately Normed Density Functional to Transition-Metal Magnetism. *Phys. Rev. Lett.* **2018**, *121*, 207201.

(39) Sun, J.; Remsing, R. C.; Zhang, Y.; Sun, Z.; Ruzsinszky, A.; Peng, H.; Yang, Z.; Paul, A.; Waghmare, U.; Wu, X.; Klein, M. L.; Perdew, J. P. SCAN: An Efficient

Density Functional Yielding Accurate Structures and Energies of Diversely-Bonded Materials. 2015.

(40) Fu, Y.; Singh, D. J. Density functional methods for the magnetism of transition metals: Scan in relation to other functionals. *Phys. Rev. B* **2019**, *100*, 045126.

(41) Perdew, J. P.; Ernzerhof, M.; Burke, K. Rationale for mixing exact exchange with density functional approximations. *J. Chem. Phys.* **1996**, *105*, 9982–9985.

(42) Viswanathan, V.; Hansen, H. A.; Rossmeisl, J.; Nørskov, J. K. Universality in Oxygen Reduction Electrocatalysis on Metal Surfaces. *ACS Catal.* **2012**, *2*, 1654–1660.

(43) Greeley, J.; Jaramillo, T. F.; Bonde, J.; Chorkendorff, I.; Nørskov, J. K. Computational high-throughput screening of electrocatalytic materials for hydrogen evolution. *Nat. Mater.* **2006**, *5*, 909–913.

(44) Calle-Vallejo, F.; Tymoczko, J.; Colic, V.; Vu, Q. H.; Pohl, M. D.; Morgenstern, K.; Loffreda, D.; Sautet, P.; Schuhmann, W.; Bandarenka, A. S. Finding optimal surface sites on heterogeneous catalysts by counting nearest neighbors. *Science* **2015**, *350*, 185–189.

(45) Towns, J.; Cockerill, T.; Dahan, M.; Foster, I.; Gaither, K.; Grimshaw, A.; Hazlewood, V.; Lathrop, S.; Lifka, D.; Peterson, G. D.; Roskies, R.; Scott, J. R.; Wilkins-Diehr, N. XSEDE: Accelerating Scientific Discovery. *Comput. Sci. Eng.* **2014**, *16*, 62–74.